Journal of the Ceramic Society of Japan 122 [4] 237-243 2014 Review

Development of nano-sized superparamagnetic ferrites having heat generation ability in an AC magnetic field for thermal coagulation therapy

Hiromichi AONO†

Graduate School of Science and Engineering, Ehime University, Matsuyama 790–8577, Japan

Thermal coagulation therapy using powdered magnetic materials in an alternating (AC) magnetic field has been expected as a treatment of cancerous tissues. For nano-sized superparamagnetic particles, the magnetic energy is mainly converted to a heat generation ability by the rotation of the magnetic moment (Néel relaxation) along with the rotation of the particles (Brownian relaxation). Fe_3O_4 (magnetite) nanoparticles have been mainly investigated as the candidate material for this type of therapy. In this review, an outline of the ferrite materials having heat generation ability in the AC magnetic field is described for the application of the thermal coagulation therapy. In particular, I focused on the preparation of a nano-sized magnetic material using physical bead milling to develop a magnetic material of $Y_3Fe_5O_{12}$ and its high heat generation ability. The preparation of $Y_3Fe_5O_{12}$ microspheres with a 20–32 μm diameter range using the bead-milled powder was also described for the embolization method of cancer treatment.

Key-words : Magnetic materials, Thermal coagulation therapy, AC magnetic field, Nanoparticle, Magnetite, $Y_3Fe_5O_{12}$, Bead milling

[Received January 4, 2014; Accepted February 19, 2014]

1. Introduction

In general, hyperthermia (also called thermal therapy) is a type of cancer treatment in which body tissue is exposed to high temperatures (up to 42–43°C) using a high frequency voltage because cancer cells can undergo damage at this temperature while normal cells remain unaffected.[1] The device for cancer therapy using a radio frequency (8 MHz) has been commercialized as the "Thermotron RF8" from Yamamoto Vinyter Co., Ltd.[2]

For local therapy, the method using powdered magnetic materials in an AC magnetic field has been expected as a treatment of cancerous tissues.[3] A drug delivery system (DDS) using nano-sized magnetic particles encapsulated in a liposome with an antibody (<100 nm) is possible as a cancer therapy in the future (**Fig. 1**). **Figure 2** shows the approximate heat generation mechanism for the superparamagnetic materials. The reason for the heat generation is attributed to the hysteresis loss in the B–H curve for ferromagnetic and ferrimagnetic materials having large particle size.[4),5] For a superparamagnetic material having a nano-sized particle size, the Néel relaxation and the Brownian relaxation become a calorigenic cause.[6)–12] For the Néel relaxation and the Brownian relaxation, the energy losses are due to the magnetic moment rotation within the crystal and the particle rotation in the dispersed solvent, respectively. The energy losses (heat generation ability) of the superparamagnetic nanoparticles due to the Néel relaxation and Brownian relaxation are proportional to the square of the magnetic field (H^2) and its frequency (f). The equation is simply expressed as:

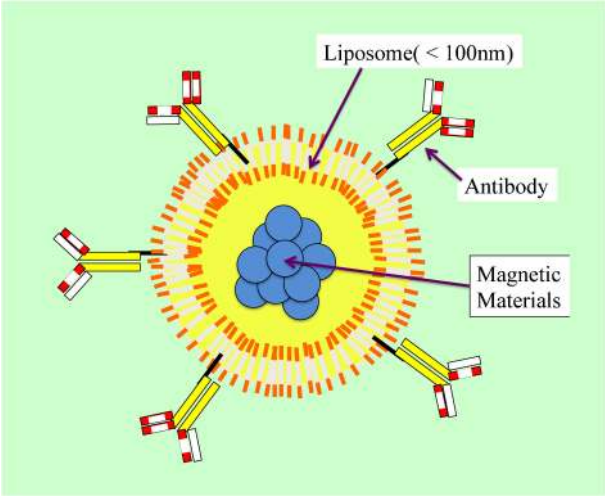

Fig. 1. DDS application of thermal coagulation therapy for cancer tumors.

$$\text{Heat generation ability } (W \cdot g^{-1}) = k \cdot f \cdot H^2 \qquad (1)$$

where k, f, and H are a constant value, frequency (kHz), and magnetic field ($kA \cdot m^{-1}$), respectively. In general, the nano-sized materials have been synthesized by a chemical method such as coprecipitation. The bead-milling as a physical method was also effective for the preparation of the nano-sized particles.

As another type of magnetic material, a microsphere for the embolization of blood vessels can be considered as one of the methods for cancer treatment. The microspheres also act to block the bloodstream (nourishment) of a cancer tumor. Radioactive ^{90}Y containing microspheres using TheraSphere® and SIR-

† Corresponding author: H. Aono; E-mail: aono.hiromichi.mf@ehime-u.ac.jp

‡ Preface for this article: DOI http://dx.doi.org/10.2109/jcersj2.122.P4-1

DOI http://dx.doi.org/10.2109/jcersj2.122.237

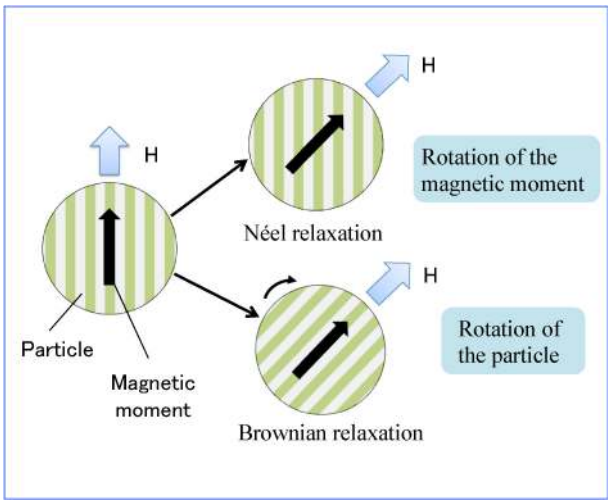

Fig. 2. Heat generation mechanism for powdered superparamagnetic magnetic materials.

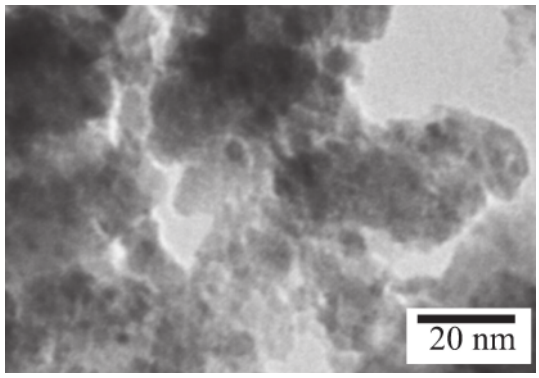

Fig. 3. TEM photo of Fe_3O_4 powder prepared by bead milling (using 0.1 mmϕ beads for 6 h).

Sphere® have already been used for the radioembolization of liver tumors.[13),14)] For the thermal coagulation therapy, the magnetic materials containing glass ceramics have been studied for the embolization method. Fe_3O_4 microspheres with a 20–30 µm diameter range were synthesized by melting the powder in a high frequency induction thermal plasma at high temperature and by precipitation from an aqueous solution.[15)] As a conventional method, the preparation of microspheres was possible by a spray drying technique at low temperature using nanoparticles.

In this review, the preparation of nano-sized superparamagnetice magnetic materials using a chemical method and physical bead-milling for the treatment of cancerous tissues is described. Furthermore, the preparation of the microspheres for the embolization method is also mentioned.

2. MFe_2O_4 type ferrite materials (M = divalent cation)

Ferrites are usually iron-containing ferrimagnetic oxides, such as MFe_2O_4, $MFe_{12}O_{19}$ (M = divalent cation) and $R_3Fe_5O_{12}$ (R = rare earth). Many ferrites have been reported as heat generation materials in AC magnetic field. A magnetite (Fe_3O_4) nanoparticle has been mainly investigated as the candidate material for this application, because the nano-sized Fe_3O_4 particles can be easily prepared in a solution at low temperature by a chemical method involving a conventional coprecipitation method as the reaction ($Fe^{2+} + 2Fe^{3+} + 8OH^- \rightarrow Fe_3O_4 + 4H_2O$).[16)–23)] An additional reason for the utilization of the magnetite is a good biocompatibility, because an agent containing the magnetite has been commercialized for contrast-enhanced MRI.[24)] The maximum increasing temperature in an AC magnetic field is for a particle with a 13-nm crystal diameter.[23)] For other ferrite materials, nano-sized M=Mn, Co, Ni, Zn materials have been reported as having particle-size dependence regarding the heat generation properties.[25)–33)] These ferrites have considerably higher Curie temperatures (Tc) than 42–43°C. To allow a self-regulated temperature for the thermal therapy, the Tc value was controlled using ion substitution into the ferrites, i.e., the $Mn_{1-x}Zn_xFe_{2-y}Gd_yO_4$ system and the $Mg_{1+x}Fe_{2-2x}Ti_xO_4$ system.[34),35)]

In the case of a ferrimagnetic material having a large particle size (particle size: several µm), $MgFe_2O_4$ has the highest heating ability of the various commercial ferrites of MFe_2O_4 (M=Mg, Mn, Fe, Co, Ni, Cu, and Sr).[36),37)] Furthermore, a higher heat generation ability was reported for the Ca^{2+} substituted $Mg_{1-X}Ca_XFe_2O_4$ system when compared to that of Fe_3O_4.[38),39)] The chemical method, such as the coprecipitation method was utilized for the preparation of the superparamagnetic nano-sized materials. However, a heat treatment involving the decomposition of the precursors is necessary for the chemical method in order to obtain these ferrite materials, except for Fe_3O_4. This calcination process decreases the dispersibility of the particles.

The physical milling of the nano-sized material is very effective for all the ferrite materials. The heat generation ability in an AC magnetic field was studied for fine Fe_3O_4 and $MgFe_2O_4$ powders that were physically prepared using the bead-milling method.[40),41)] In the case of Fe_3O_4, the starting material using a commercial powder sample of ca. 2.0 µm in particle size showed a poor heat generation ability in an AC magnetic field. The heat generation ability in the AC magnetic field improved with the milling time, i.e., due to a decrease in the average particle size. The highest heat ability in the AC magnetic field was for a fine Fe_3O_4 powder with a 17-nm particle size (the samples were milled for 6 h using 0.1 mmϕ beads). The particle size was estimated based on the surface area. A TEM image is shown in **Fig. 3**. However, the heat generation ability decreased for the excessively milled Fe_3O_4 samples having average particle sizes.

To study the mechanism of the heat generation for the best sample, the heat generation ability ($W \cdot g^{-1}$) was quantitatively measured for three different methods (**Fig. 4**), (a) a magnetic material powder (2.0 g) with 10 ml of water, (b) a hardened magnetic material powder sample (2.0 g) with 10 ml of water using agar, and (c) solidified samples containing the magnetic material powder (2.0 g) using an epoxy resin adhesive with 10 ml of water. Air was slowly bubbled into the glass container for stirring the water for (a) and (c) in order to have the same temperature distribution and the homogeneous magnetic material particle dispersion for (a). In this measurement, the heat generation ability was calculated using the temperature enhance ratio ($dT/dt = K \cdot s^{-1}$) for the initial 5 min using the following equation:

$$\text{Heat generation ability } (W \cdot g^{-1}) = C \cdot (dT/dt)/M \quad (2)$$

where M and C are the sample weight (g), and the estimated total heat capacity ($J \cdot K^{-1}$) of 10 ml of water with the contact glass of the glass container, respectively.

Figure 5 shows the relationship between the square of the magnetic field (H^2) and heat generation ability for the three types

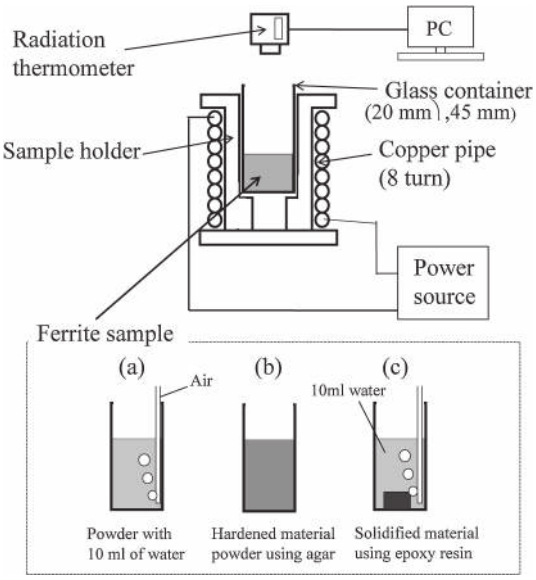

Fig. 4. Apparatus for measuring the heat generation ability. The samples for the measurement of the heat generation ability, (a) ferrite powder (2.0 g) with 10 ml of water, (b) hardened ferrite powder (2.0 g) with 10 ml of water using agar, (c) solidified ferrite powder (2.0 g) using epoxy resin.

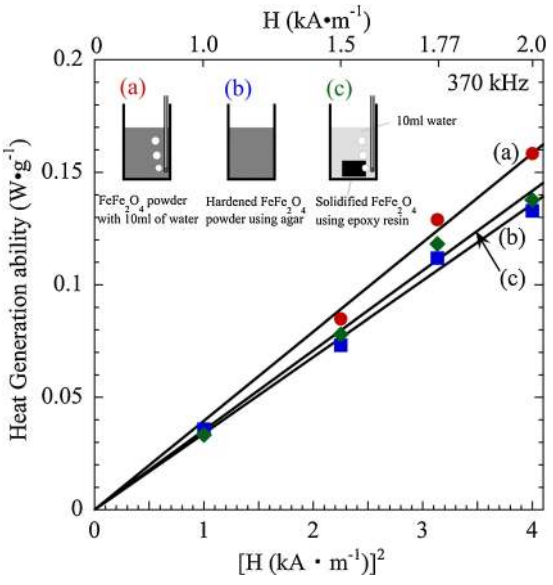

Fig. 5. Relationship between the square of the magnetic field (370 kHz) and heat generation ability for Fe_3O_4 powder prepared by bead milling (using 0.1 mmϕ beads for 6 h). Three types of samples, (a) Fe_3O_4 powder with 10 ml of water, (b) hardened Fe_3O_4 powder with 10 ml of water using agar, (c) solidified Fe_3O_4 powder using epoxy resin.

of samples. The energy losses for all the samples were proportional to the square of the magnetic field. **Figure 6** plots the relationship between the frequency of the AC magnetic field (150–370 kHz, 1.77 kA·m^{-1}) and heat generation ability for the three types of methods. The energy losses for all the samples were proportional to the frequency of the AC magnetic field. It was reported that the energy losses (heat generation ability) of magnetite nanoparticles due to the Néel relaxation and Brownian relaxation are proportional to the square of the magnetic field (H^2) and its frequency (f). The result of using sample (a) in water is due to the total energy loss of the Néel relaxation and the

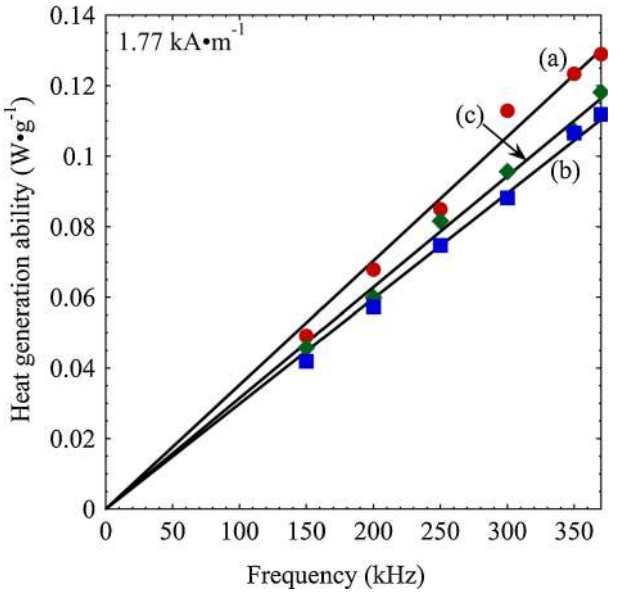

Fig. 6. Relationship between frequency of the AC magnetic field (150–370 kHz, 1.77 kA·m^{-1}) and heat generation ability for Fe_3O_4 powder prepared by bead milling using 0.1 mmϕ beads for 6 h. Three types of samples, (a) Fe_3O_4 powder with 10 ml of water, (b) hardened Fe_3O_4 powder with 10 ml of water using agar, and (c) solidified Fe_3O_4 powder using epoxy resin.

Brownian relaxation. The estimated k value in Eq. (1) using the result was 1.07×10^{-4} for the total loss of this sample having the best heat generation ability. When the heat generation of sample (a) was compared to that of sample (b), this difference (ca. 8%) would be due to the Brownian relaxation, because the particle rotation could not occur in the hardened sample containing the agar. The main reason for the high heat generation properties of the milled samples was ascribed to an increase in the Néel relaxation of the superparamagnetic material. The energy loss of the solidified sample (c) using epoxy resin was almost the same as that of sample (b). This means that the concentration of the ferrite in the sample does not affect the heat generation ability in an AC magnetic field.[40]

3. $Y_3Fe_5O_{12}$

3.1 Preparation using bead milling

The maximum heat generation ability was obtained for $Y_3Fe_5O_{12}$ in the ferrimagnetic $R_3Fe_5O_{12}$ (R=Y, Sm, Gd, Dy, Ho, Er) powder material synthesized by a reverse coprecipitation method and calcination at 1100°C.[42),43)] The bead-milled $Y_3Fe_5O_{12}$ ferrite also had a high heat generation ability in the nano-sized superparamagnetic materials.[44),45)] The maximum heat generation was obtained for the samples milled for 4 h using the 0.1 mmϕ beads having an ca. 15 nm crystallite size and ca. 26 nm particle size. The particle size was 1.5–2 times greater than the crystallite size for all the samples due to the cohesion of the small crystallites which resulted in larger particles. The heat generation ability decreased with a decrease in the particle diameter below ca. 26 nm.

Figure 7 shows the relationship between the square of the magnetic field (H^2) and the heat generation ability for the three types of methods as shown in Fig. 4 for the bead-milled $Y_3Fe_5O_{12}$ ferrite having the maximum heat generation ability. The energy losses for all the samples were proportional to the square of the magnetic field. For these samples, the energy losses

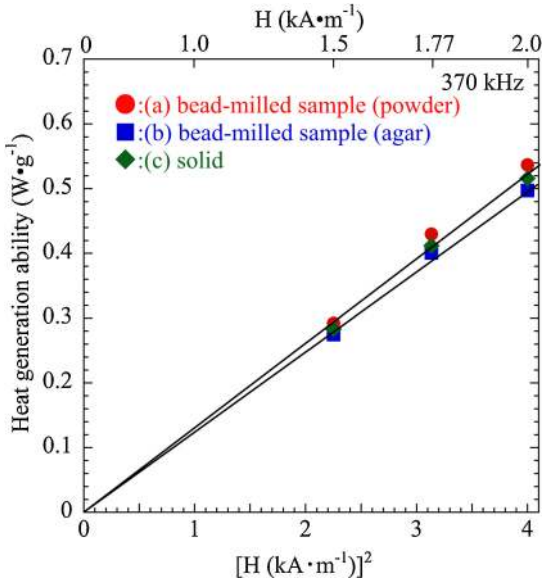

Fig. 7. Relationship between the square of the magnetic field (370 kHz) and heat generation ability for three types of (Fig. 4) $Y_3Fe_5O_{12}$ powder samples prepared by bead milling (using 0.1 mmϕ beads for 4 h).

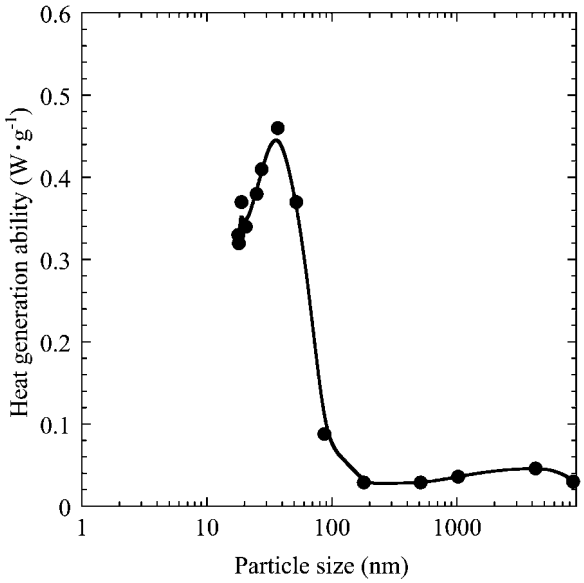

Fig. 8. Relationship between the particle size and heat generation ability for calcined $Y_3Fe_5O_{12}$ powders at various temperatures.

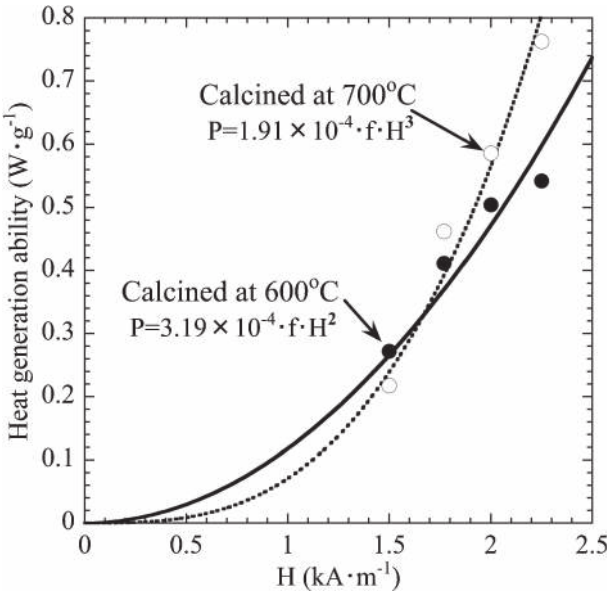

Fig. 9. Relationship between the magnetic field (370 kHz) and heat generation ability of two types of calcined $Y_3Fe_5O_{12}$ powders at 600 and 700°C.

for all the samples were also proportional to the frequency of the AC magnetic field. The result of a sample (a) in water is a total energy loss value. The estimated k value in Eq. (1) using these results was 3.58×10^{-4} for the total loss of this sample having the best heat generation ability. When the heat generation of sample (a) was compared to that of sample (b), this difference due to the Brownian relaxation was 5–6%. The main reason for the high heat generation property of the milled samples was ascribed to an increase in the Néel relaxation. For this sample, the concentration of the ferrite in the sample does not affect the heat generation ability in an AC magnetic field because of close heat abilities of the (b) and (c) samples.

3.2 Effect of calcination at low temperature

Heterogeneous particles should be obtained by the physical bead-milling which would influence the heat generation ability. To confirm the effect of the calcination, $Y_3Fe_5O_{12}$ powder was thoroughly bead-milled using 0.05 mmϕ beads for 10 h. The particle size of the obtained powder was 20.5 nm which is smaller than ca. 26 nm of the sample having the highest heat ability milled for 4 h using 0.1 mmϕ beads.[46] The Néel relaxation was reduced by the excessive bead-milling using small beads for 10 h. The effect of particle growth on the heat generation ability was studied for the samples calcined at low temperature. **Figure 8** plots the relationship between the particle diameter and heat generation ability. The heat generation ability was improved with an increase in the particle size. The maximum heat generation ability in an AC magnetic field was obtained for the sample calcined at 700°C (particle size: ca. 35 nm). The heat generation was strongly reduced with the increase in an particle size for the samples sintered at higher temperatures. **Figure 9** shows the relationship between the magnetic field (370 kHz) and the heat generation ability for the samples calcined at 600 and 700°C. The energy losses were proportional to the square and cube of the magnetic field for the samples calcined at 600 and 700°C, respectively. It was confirmed that the heat generation ability for all the samples was proportional to the frequency of the AC magnetic field. For the samples calcined at 600°C and lower temperatures, these superparamagnetic samples were proportional to the square of the magnetic field as shown in Eq.(1). On the other hand, the heat generation ability of the samples calcined at 700°C and higher temperatures was proportional to the cube of the magnetic field (H^3) for the ferrimagnetic sample.[47] For the sample calcined at 700°C, the heat generation ability is expressed by the following equation:

$$\text{Heat generation ability } (\text{W} \cdot \text{g}^{-1}) = 1.91 \times 10^{-4} \cdot \text{f} \cdot \text{H}^3 \quad (3)$$

where f and H are the frequency (kHz) and the magnetic field (kA·m^{-1}), respectively. The heat generation mechanism in the AC magnetic field changed due to the calcination at 700°C from superparamagnetism to ferrimagnetism. A higher heat generation

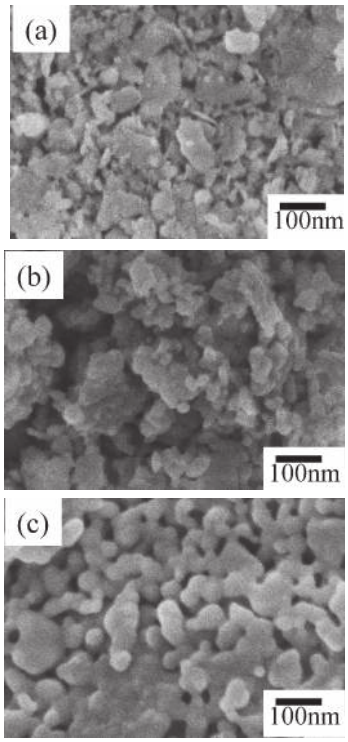

Fig. 10. SEM images for bead-milled $Y_3Fe_5O_{12}$ of (a) non-calcined sample and the samples calcined (b) at 650°C and (c) 800°C.

ability was obtained for the $Y_3Fe_5O_{12}$ sample calcined at 700°C for the ferrimagnetic materials above 1.6 kA·m^{-1}. The boundary between the superparamagnetic and ferrimagnetic materials was ca. 30–35 nm in particle size for $Y_3Fe_5O_{12}$. This diameter agreed with the upper limit (35 nm) of the superparamagnetic behavior of the $Y_3Fe_5O_{12}$ prepared by a sol–gel method.[48)]

Figure 10 shows SEM observation for the (a) non-calcined sample and the samples calcined (b) at 650°C and (c) 800°C. The particles in the non-calcined sample had a heterogeneous shape with many sharp edges due to the aggregation of the nano-sized particles. The homogeneity of the particles with a round shape was improved with an increase in the calcination temperature.[49)]

The calcined samples at low temperature were also studied for the bead-milled (0.05 mmϕ beads for 10 h) nano-sized $Y_3Fe_5O_{12}$–$n$$SmFeO_3$ mixed powders. The calcination temperature for the change in the mechanism was increased to 800°C for the $n =$ 0.2 sample. The $SmFeO_3$ addition caused an increase in the calcination temperature for the formation of the ferrimagnetic material due to the decreased particle growth. The calcination temperature for the ferrimagnetic material was increased to 900 and 1000°C for $n = 0.4$ and $n = 0.6$, respectively.[50)]

3.3 Preparation of microspheres for embolization method

For the embolization method used for the cancer therapy, the preparation of $Y_3Fe_5O_{12}$ microspheres with a 20–32 µm diameter range was investigated by the spray-drying method using the bead-milled nano-sized particles. The preparation of microspheres using a spray-dry method has been specifically reported for organic materials such as chitosan for colonic drug delivery.[51),52)] Bead-milled $MgFe_2O_4$ and $Y_3Fe_5O_{12}$ were tested for the preparation of microspheres using the spray-drying method.[53),54)] **Figure 11** shows a spray-drier used for the preparation of the microspheres. The slurry for the spray-drier was obtained as a

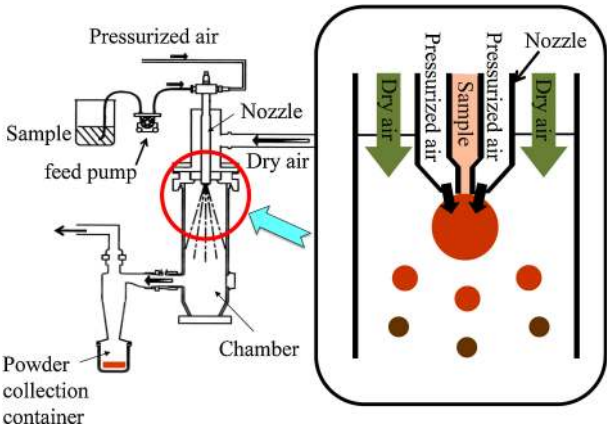

Fig. 11. The spray dryer apparatus for preparation of ferrite microspheres.

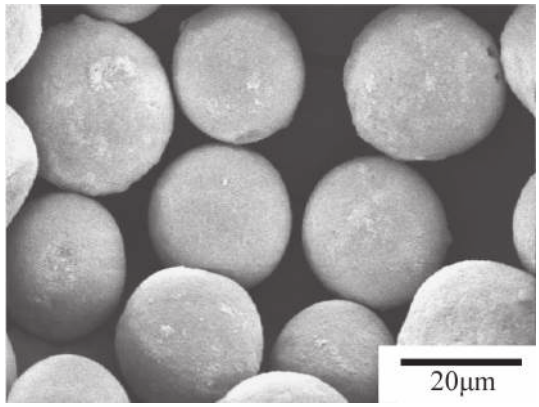

Fig. 12. SEM photos of the spray dried particles after sifting.

mixture of the bead-milled $Y_3Fe_5O_{12}$ and purified water, and then sprayed by heated air at 200°C as small droplets by the spray-drier with an nozzle atomizer. The droplets were isotropically dried in the chamber to form ferrite microspheres. The spray-dried powder was washed using purified water on a 32-µm sieve to screen out the larger particles. The sifted slurry containing the particles under 32-µm and purified water was then thoroughly washed on a 20-µm sieve to remove any smaller particles. The powder on the 20-µm sieve, which contained the 20–32 µm particles, was then dried at 100°C.

Figure 12 shows SEM photos of the spray dried particles after the sifting. The homogeneous microspheres of 20–32 µm in size were obtained using the spray-dry method and the sifting. These microspheres are formed by the cohesive power of the bead-milled nano-sized powder. **Figure 13** shows the relationship between the square of the AC magnetic field (H^2) (370 kHz) and the heat generation ability for the bead-milled sample and microsphere sample. The energy losses for both materials were proportional to the square of the magnetic field. The heat generation ability of the microsphere sample was close to that for the bead-milled sample. A low temperature treatment at 200°C using the spray-drier for the preparation of the microspheres did not influence the heat generation ability. The energy losses for both samples were also proportional to the frequency of the AC magnetic field. The result of the bead-milled sample in water is the total energy loss value of the Néel relaxation and Brownian relaxation. The estimated k value in Eq. (1) using these results was 3.50×10^{-4} for the total loss of this sample having the best

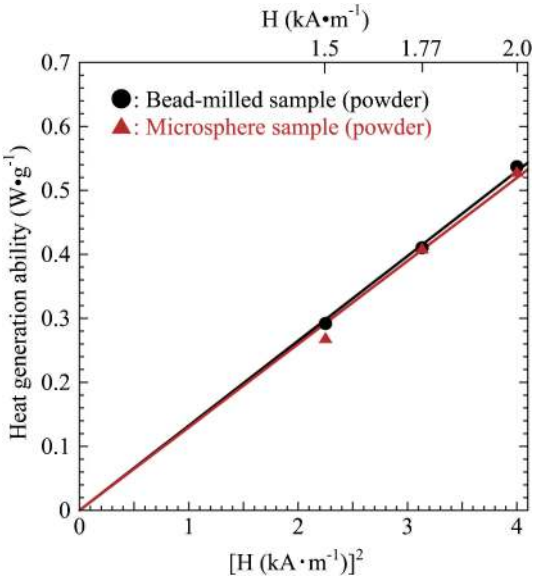

Fig. 13. Relationship between the square of the magnetic field (370 kHz, 1.5–2.0 kA·m^{-1}) and heat generation ability for (a) the bead-milled $Y_3Fe_5O_{12}$ powder samples (using 0.1 mmϕ beads for 4 h) and (b) the microsphere sample.

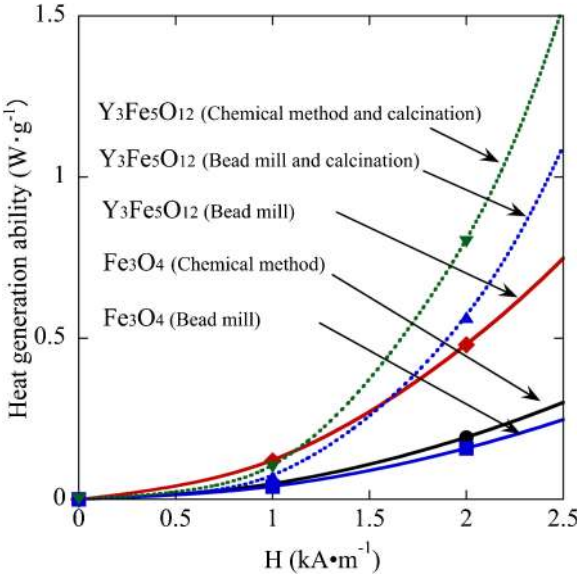

Fig. 14. Comparison of the relationship between the magnetic field (370 kHz) and the heat generation ability (W·g^{-1}) for the typical samples.

Table 1. Comparison of heat generation ability in an AC magnetic field for typical ferrite materials

Sample	Preparation method	Calcination temp. (°C)	Particle dia. (nm)	Heat generation ability (W·g^{-1})	Ref.
Fe_3O_4	Chemical method	—	13	1.29×10^{-4} f·H^2	23)
Fe_3O_4	Bead mill	—	17	1.07×10^{-4} f·H^2	40)
$Y_3Fe_5O_{12}$	Bead mill	—	26	3.58×10^{-4} f·H^2	45)
$Y_3Fe_5O_{12}$	Bead mill	700	35	1.91×10^{-4} f·H^3	46)
$Y_3Fe_5O_{12}$	Chemical method	1100	1520	2.70×10^{-4} f·H^3	43)

heat generation ability. The heat generation for the Brownian relaxation of the particle rotation could be ignored for the microsphere sample, because the particle rotation hardly occurred for the large microspheres. This result also suggested that the main reason for the high heat generation property of the milled samples was an increase in the Néel relaxation.

4. Comparison of heat generation for the ferrites

Figure 14 compares the heat generation ability in the AC magnetic field (370 kHz), of typical materials, i.e., (i) the Fe_3O_4 nanoparticle prepared by the chemical method,[23] (ii) the bead milled Fe_3O_4 nanoparticle,[40] (iii) the bead-milled $Y_3Fe_5O_{12}$ sample,[45] (iv) a calcined $Y_3Fe_5O_{12}$ powder at 700°C after bead milling,[46] and (v) the $Y_3Fe_5O_{12}$ sample prepared by calcination at 1100°C for the precursor by a chemical method.[43] **Table 1** lists the particle diameter and the heat generation ability for these ferrite powders. The heat ability increased as a function proportional to the square or cube with an increase in the magnetic The heat generation ability of the (i) Fe_3O_4 nanoparticle prepared using the chemical method is the standard value because of the candidate material for this application. For the nano-sized superparamagnetic materials (i)–(iii), the heat generation ability was proportional to the frequency and the square of the magnetic field (H^2) and the highest heat generation ability was obtained for (iii) the bead-milled $Y_3Fe_5O_{12}$. The maximum heat ability was obtained for the bead-milled $Y_3Fe_5O_{12}$ below 1.2 kA·m^{-1}. In a higher magnetic field, the $Y_3Fe_5O_{12}$ prepared by the chemical method and calcination showed the maximum heat ability, because the ferrimagnetic material performance was proportional to the cube of the magnetic field (H^3). However, the particle size for this ferrimagnetic material was too large to use in DDS applications. Based on these comparisons, the bead-milled $Y_3Fe_5O_{12}$ prepared in this study is the best material for these applications.

5. Conclusions

The preparation of nano-sized superparamagnetic magnetic materials using a chemical method and physical bead-milling for the treatment of cancerous tissues has been desribed. Fe_3O_4 nanoparticles have been mainly investigated as the candidate material for this application, because the preparation of this material is easily prepared in a solution at low temperature by a conventional coprecipitation method. The heat generation ability of 3.58×10^{-4} fH^2 (W·g^{-1}) for the $Y_3Fe_5O_{12}$ ferrite materials in an AC magnetic field knowing the arbitrary frequency (f/kHz) and the magnetic field (H/kA·m^{-1}) showed the best heat generation ability of the reported superparamagnetic materials. This means that the heat generation in the cancer tumor can be controlled using the arbitrary frequency (f/kHz) and the magnetic field (H/kA·m^{-1}). Furthermore, the $Y_3Fe_5O_{12}$ microspheres having a high heat generation ability were applicable for the thermal coagulation therapy using the embolization method.

References

1) W. C. Dewey, L. E. Hopwood, S. A. Sapareto and L. E. Gerweck, *Radiology*, 123, 463–474 (1977).
2) M. Abe, M. Hiraoka, M. Takahashi, S. Egawa, C. Matsuda, Y.

Onoyama, K. Morita and M. Kakehi, *Cancer*, 58, 1589–1595 (1986).
3) A. Jordan, R. Scholz, P. Wust, H. Fähling and R. Felix, *J. Magn. Magn. Mater.*, 201, 413–419 (1999).
4) M. Ma, Y. Wu, J. Zhou, Y. Sun, Y. Zhang and N. Gu, *J. Magn. Magn. Mater.*, 268, 33–39 (2004).
5) A. Jordan, P. Wust, H. Fähling, W. John, A. Hinz and R. Felix, *Int. J. Hyperthermia*, 9, 51–68 (1993).
6) R. Hergt, W. Andrä, C. G. D'Ambly, I. Hilger, W. A. Kaiser, U. Richter and H. Schmidt, *IEEE Trans. Magn.*, 34, 3745–3754 (1998).
7) R. E. Rosensweig, *J. Magn. Magn. Mater.*, 252, 370–374 (2002).
8) J. Fortin, C. Wilhelm, J. Servais, C. Ménager, J. Bacri and F. Gazeau, *J. Am. Chem. Soc.*, 129, 2628–2635 (2007).
9) T. Atsumi, B. Jeyadevan, Y. Sato and K. Tohji, *J. Magn. Magn. Mater.*, 310, 2841–2843 (2007).
10) B. Jeyadevan, *J. Ceram. Soc. Japan*, 118, 391–401 (2010).
11) J.-H. Lee, J.-T. Jang, J.-S. Choi, S. H. Moon, S. Noh, J. Kim, J.-G. Kim, K. I. Park and J. Cheon, *Nat. Nanotechnol.*, 6, 418–422 (2011).
12) H. Miyama, *J. Nanomaterials*, art. no. 752973 (2013).
13) R. Murthy, R. Nunez, F. Szklaruk, W. Erwin, D. C. Madoff, S. Gupta, K. Ahrar, M. F. Wallace, A. Cohen, D. M. Coldwell, A. S. Kennedy and M. E. Hicks, *Radiographics*, 25[SPEC. ISS.], S41–S55 (2005).
14) R. Salem, R. J. Lewandowski, B. Atassi, S. C. Gordon, V. L. Gates, O. Barakat, Z. Sergie, C.-Y. Wong and K. G. Thurston, *J. Vasc. Interv. Radiol.*, 16, 1627–1639 (2005).
15) M. Kawashita, M. Tanaka, T. Kokubo, Y. Inoue, Y. Takeshi, S. Hamada and T. Shinjo, *Biomaterials*, 26, 2231–2238 (2005).
16) A. Jordan, R. Scholz, K. Maier-Hauff, M. Johannsen, P. Wust, J. Nadobny, H. Schirra, H. Schmidt, S. Deger, S. Loening, W. Lanksch and R. Felix, *J. Magn. Magn. Mater.*, 225, 118–126 (2001).
17) P. Moroz, S. K. Jones and B. N. Gray, *Int. J. Hyperthermia*, 18, 267–284 (2002).
18) A. Ito, M. Shinkai, H. Honda and T. Kobayashi, *J. Biosci. Bioeng.*, 100, 1–11 (2005).
19) M. Johannsen, U. Gneveckow, B. Thiesen, K. Taymoorian, C. H. Cho, N. Waldöfner, R. Scholz, A. Jordan, S. A. Loening and P. Wust, *Eur. Urol.*, 52, 1653–1662 (2007).
20) K. Maier-Hauff, R. Rothe, R. Scholz, U. Gneveckow, P. Wust, B. Thiesen, A. Feussner, A. Deimling, N. Waldoefner, R. Felix and A. Jordan, *J. Neurooncol.*, 81, 53–60 (2007).
21) K. Hayashi, W. Sakamoto and T. Yogo, *J. Magn. Magn. Mater.*, 321, 450–457 (2009).
22) M. Yoshida, Y. Watanabe, M. Sato, T. Maehara, H. Aono, T. Naohara, H. Hirazawa, A. Horiuchi, S. Yukumi, K. Sato, H. Nakagawa, Y. Yamamoto, H. Sugishita and K. Kawachi, *Int. J. Cancer*, 126, 1955–1965 (2010).
23) H. Aono, H. Hirazawa, T. Naohara, T. Maehara, H. Kikkawa and Y. Watanabe, *Mater. Res. Bull.*, 40, 1126–1135 (2005).
24) P. Reimer and T. Balzer, *Eur. Radiol.*, 13, 1266–1276 (2003).
25) M. Kawashita, Y. Iwahashi, T. Kokubo, T. Yao, S. Hamada and T. Shinjo, *J. Ceram. Soc. Japan*, 112, 373–379 (2004).
26) P. Pradhan, J. Giri, G. Samanta, H. D. Sarma, K. P. Mishra, J. Bellare, R. Banerjee and D. Bahadur, *J. Biomedical Materials Reseach-Part B Applied Biomaterials*, 81, 12–22 (2007).
27) S. W. Lee, S. Bae, Y. Kakemura, I.-B. Shim, T. M. Kim, J. Kim, H. J. Lee, S. Zurn and C. S. Kim, *J. Magn. Magn. Mater.*, 310, 2868–2870 (2007).
28) G. Baldi, D. Bonacchi, C. Innocenti, G. Lorenzi and C. Sangregorio, *J. Magn. Magn. Mater.*, 311, 10–16 (2007).
29) Q. Tang, D. Zhang, X. Cong, M. Wan and L. Jin, *Biomaterials*, 29, 2673–2679 (2008).
30) B. E. Kashevsky, V. E. Agabekov, S. B. Kashevsky, K. A. Kekalo, E. Y. Manina, I. V. Prokhorov and V. S. Ulashchik, *Particuology*, 6, 322–333 (2008).
31) D.-H. Kim, D. E. Nikles, D. T. Johnson and C. S. Brazel, *J. Magn. Magn. Mater.*, 320, 2390–2396 (2008).
32) A. Tomitaka, A. Hirukawa, T. Yamada, S. Morishita and Y. Takemura, *J. Magn. Magn. Mater.*, 321, 1482–1484 (2009).
33) I. Sharifi, H. Shokrollahi and S. Amiri, *J. Magn. Magn. Mater.*, 324, 903–915 (2012).
34) T. N. Brusentsova, N. A. Brusentov, V. D. Kurnetsov and V. N. Nikiforov, *J. Magn. Magn. Mater.*, 293, 298–302 (2005).
35) G. Ferk, M. Drofenik, D. Lisjak, A. Hamler, Z. Jaglicic and D. Makovec, *J. Magn. Magn. Mater.*, 350, 124–128 (2014).
36) T. Maehara, K. Konishi, T. Kamimori, H. Aono, T. Naohara, H. Kikkawa, Y. Watanabe and K. Kawach, *Jpn. J. Appl. Phys.*, 41, 1620–1621 (2002).
37) T. Maehara, K. Konishi, T. Kamimori, H. Hirazawa, H. Aono, T. Naohara, S. Nomura, H. Kikkawa, Y. Watanabe and K. Kawachi, *J. Mater. Sci.*, 40, 135–138 (2005).
38) H. Aono, H. Hirazawa, T. Ochi, T. Naohara, K. Mori, Y. Hattori, T. Maehara, H. Kikkawa and Y. Watanabe, *Chem. Lett.*, 34, 482–483 (2005).
39) H. Hirazawa, S. Kusamoto, H. Aono, T. Naohara, K. Mori, Y. Hattori, T. Maehara and Y. Watanabe, *J. Alloys Compd.*, 461, 467–473 (2008).
40) H. Aono, Y. Watanabe, T. Naohara, T. Maehara, H. Hirazawa and Y. Watanabe, *Mater. Chem. Phys.*, 129, 1081–1088 (2011).
41) H. Hirazawa, H. Aono, T. Naohara, T. Maehara and Y. Watanabe, *J. Magn. Magn. Mater.*, 323, 675–680 (2011).
42) T. Nishimori, T. Naohara, T. Maehara, H. Hirazawa and H. Aono, *J. Iron Steel Res. Int. (Proc. of EPM2012)*, 19[Suppl. 1], 600–603 (2012).
43) H. Aono, K. Moritani, T. Naohara, T. Maehara, H. Hirazawa and Y. Watanabe, *Mater. Lett.*, 65, 1454–1456 (2011).
44) H. Aono, H. Ebara, R. Senba, T. Naohara, T. Maehara, H. Hirazawa and Y. Watanabe, *J. Am. Ceram. Soc.*, 94, 4116–4119 (2011).
45) H. Aono, H. Ebara, R. Senba, T. Naohara, T. Maehara, H. Hirazawa and Y. Watanabe, *J. Magn. Magn. Mater.*, 324, 1985–1991 (2012).
46) T. Nishimori, Y. Akiyama, T. Naohara, T. Maehara, H. Hirazawa and H. Aono, *J. Ceram. Soc. Japan*, 121, 13–16 (2013).
47) L. Rayleigh, *Philos. Mag.*, 23, 225–248 (1887).
48) R. D. Sánchez, J. Rivas, P. Vaqueiro, M. A. López-Quintela and D. Caeiro, *J. Magn. Magn. Mater.*, 247, 92–98 (2002).
49) H. Aono, R. Senba, T. Nishimori and T. Naohara, *J. Am. Ceram. Soc.*, 96, 3483–3488 (2013).
50) T. Nishimori, Y. Akiyama, T. Naohara, T. Maehara, H. Hirazawa, Y. Itagaki and H. Aono, *J. Ceram. Soc. Japan*, 122, 35–39 (2014).
51) M. L. Lorenzo-Lamosa, C. Remuñán-López, J. L. Vila-Jato and M. J. Alonso, *J. Controlled Release*, 52, 109–118 (1998).
52) P. He, S. S. Davis and L. Illum, *Int. J. Pharm.*, 187, 53–65 (1999).
53) H. Aono, T. Naohara, T. Maehara, H. Hirazawa and Y. Watanabe, *J. Ceram. Soc. Japan*, 118, 1207–1211 (2010).
54) H. Aono, R. Senba, T. Nishimori and T. Naohara, *J. Am. Ceram. Soc.*, 96, 3483–3488 (2013).